Journal of Materials Chemistry A

Accepted Manuscript

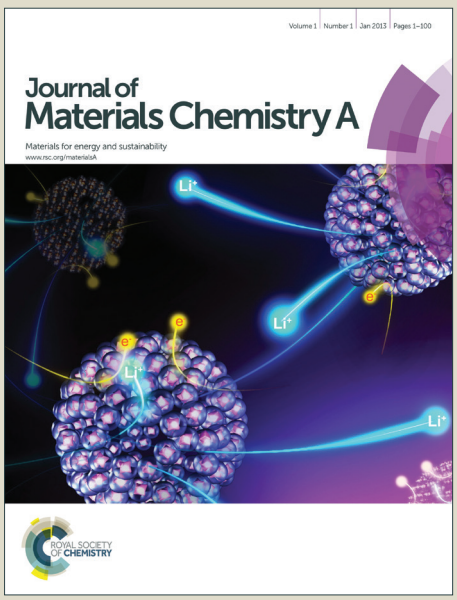

ROYAL SOCIETY OF CHEMISTRY

www.rsc.org/materialsA

Journal Name
Journal of Materials Chemistry A
Dynamic Article Links ►

Cite this: DOI: 10.1039/c0xx00000x

www.rsc.org/xxxxxx

ARTICLE TYPE

Effects of La fluoride and La hydride on the reversible hydrogen sorption behaviors in $NaBH_4$: A comparison study

Lina Chong [a], Jianxin Zou [a,b*], Xiaoqin Zeng [a,b], Wenjiang Ding [a,b]

Received (in XXX, XXX) Xth XXXXXXXXX 20XX, Accepted Xth XXXXXXXXX 20XX
DOI: 10.1039/b000000x

In the present work, two new reversible hydrogen storage composites, $NaBH_4$+LaF_3 and $NaBH_4$+LaH_2, were prepared through mechanical milling method with the aim of studying comparatively the effects of La fluoride and La hydride on the hydrogen sorption behaviors in $NaBH_4$. Experimental investigations have shown that both La fluoride and La hydride enable the reversible hydrogen sorption in $NaBH_4$. In particular, LaF_3 exhibits a superior promoting effect than LaH_2, which agrees well with the theoretical predictions. Surprisingly, better hydrogen sorption properties can be achieved in both systems through undergoing de-/rehydriding cycles. The reversible hydrogen storage capacity reaches up to 3.0 wt% at 238 ^oC and 2.9 wt% at 326 ^oC in $NaBH_4$+LaF_3 and $NaBH_4$+LaH_2 systems after the 6th dehydrogenation, respectively. In both cases, the formation of La boride plays the major role for the reversible hydrogen sorption in $NaBH_4$. The superior promoting effect of La fluoride over La hydride upon modifications of thermodynamics and kinetics of $NaBH_4$ should be ascribed to the following factors: i) The formation of thermodynamically more stable compound NaF instead of NaH reduces the overall enthalpy changes of re/de-hydriding reactions in $NaBH_4$+LaF_3 to -31.8 kJ mol^{-1} H_2 and 72.5 kJ mol^{-1} H_2, respectively; ii) The ion exchange of F^- for H^- leads to the reduction of the onset dehydrogenation temperature of $NaBH_4$ to 160 ^oC in the $NaBH_4$+LaF_3 composite; iii) F^- anion favors the formation of LaB_6 while H^- favors the formation of LaB_4. The role of the functional anions and cations, de-/rehydrogenation mechanisms and nucleation modes in the two reversible hydrogen storage composites have been proposed based on experimental and theoretical analyses. The comparison study carried out in this work helps to design and search for new metal borohydrides based composites for reversible hydrogen storage.

1. Introduction

Hydrogen is considered to be a promising fuel for future society due to its high energy density, inexhaustible resources and cleanness. However, the hydrogen storage has been recognized as one of the great challenges towards the commercialization of hydrogen-powered vehicles. To meet the requirements for on-board applications, hydrogen storage carriers should have high hydrogen storage capacity, high safety with good hydrogen sorption reversibility in particular.[1] Recently, light metal borohydrides have been attracting much attention as promising hydrogen storage materials, since they have very high gravimetric capacities.[2, 3] For example, $NaBH_4$, as a prospective hydrogen storage material, has a theoretical hydrogen capacity of 10.6 wt% upon dissociation into Na + B. However, the desorption of $NaBH_4$, proceeds at temperature as high as 500 ^oC, with NaH and $Na_2B_{12}H_{12}$ as possible intermediates.[4, 5] In addition, due to the inherent limitation to the slow diffusion of elements in the solid state, the dehydrogenation kinetics is very slow, and almost no reversibility can be achieved. Several novel strategies have been recently employed to overcome hydrogen sorption kinetic and thermodynamic limitations for $NaBH_4$, such as mechanical milling with appropriate reactants,[6-8] nano-confinement in porous scaffolds,[4] catalyst addition,[9] partial substitution of Na^+ by other metal cations.[10] All of these methods have been testified to improve the reversible hydrogen storage properties of $NaBH_4$. For example, NdF_3[6] reduces the dehydrogenation enthalpy of $NaBH_4$ by 13.6 kJ mol^{-1} H_2 compared with that of pure $NaBH_4$ (100 kJ mol^{-1} H_2),[11] which is superior to TiF_3 in the $3NaBH_4/TiF_3$ composite.[9] On the other hand, nano-confinement of $NaBH_4$ in porous carbon has also led to much faster hydrogen desorption kinetics.[4] Recently, the strategy of producing multi cation borohydrides $MM'(BH_4)_n$,[12] in which M and M' have different electronegativities, has been experimentally proved to be useful in tuning the thermodynamics of $NaBH_4$. For example, Dorthe RavnsbæK et al.[13] prepared $NaZn_2(BH_4)_5$ and $NaZn(BH_4)_3$ by mechanical milling $NaBH_4/ZnCl_2$ mixtures in appropriate molar ratios. Radovan Cerny et al. [10] successfully prepared $NaSc(BH_4)_4$ at ambient conditions in ball-milled mixtures of $NaBH_4$ and $ScCl_3$. Furthermore, nano-confinement of $NaZn(BH_4)_3$ by infusing $NaZn(BH_4)_3$ into mesoporous SBA-15 has been experimentally investigated.[14] Dehydrogenation tests show that

a Shanghai Engineering Research Center of Magnesium Materials and Application & National Engineering Research Center of Light Alloy Net Forming, Shanghai Jiao Tong University, Shanghai 200240, China
b State Key Laboratory of Metal Matrix composite & School of Materials Science and Engineering, Shanghai Jiao Tong University, Shanghai 200240, China
*Corresponding author : Jianxin Zou Tel : 86-21-54742381 ; Fax : 86-21-34203730; Email : zoujx@sjtu.edu.cn

the decomposition temperatures of these dual-cation borohydrides, especially the nano-confined $NaZn(BH_4)_3$, are lower than that of $NaBH_4$.

Recently, anion substitution has been suggested as a new approach to improve the de-/rehydrogenation thermodynamic properties of complex hydrides due to possible changes in the formation enthalpy, chemical pressure and metal–hydrogen bond strength.[15] F^- substitution for H^- was reported by Brinks et al. in Na-Al-F-H system ($Na_3AlH_{6-x}F_x$),[16] and theoretically calculations suggested a decreased enthalpy upon substitution, which was verified experimentally.[17, 18] Additionally, Yin et al. reported that the decomposition enthalpy decreased with the number of F^- substituting for H^- in $LiBH_4$ lattice.[19]

Another approach is to establish a compound known as "reactive hydride composites" (HRC), for which a metal hydride is combined with a complex hydride. For instance, MgH_2 has been successfully used by Vajo et al.[20] and Garroni et al.[21] to lower the dehydrogenation temperature of $LiBH_4$. The MgB_2 formed exothermically during an endothermic desorption is a more stable reaction product than either Mg or B, resulting in the reduced reaction enthalpy of dehydrogenation and eventually decreases the dehydrogenation temperature. However, the dehydrogenation of $2LiBH_4+MgH_2$[20] and $2NaBH_4+MgH_2$[22] composites proceeds through a two-step reaction to produce LiH/NaH and MgB_2. Therefore, it is unlikely that the dehydrogenation of these composites starts below the dehydrogenation temperature of MgH_2 (~ 288 ^oC at 1 bar of hydrogen). Currently, lanthanide hydrides showed remarkable effects on reversible dehydrogenation of $LiBH_4$, such as YH_2 and CeH_2,[23] LaH_2,[24] GdH_2,[25] especially mechanically milling $6LiBH_4$ with CeH_2 could reduce the desorption enthalpy by 16 kJ mol^{-1} compared with that of pure $LiBH_4$.[26]

In our previous studies on the reversible hydrogen storage of $3NaBH_4/NdF_3$ and $3NaBH_4/PrF_3$ systems, corresponding lanthanide hydrides have formed in the dehydrogenated samples, and may act as catalysts during de-/rehydrogenation processes. However, lanthanide hydrides as reactants working on the dehydrogenation process of $NaBH_4$ has not been investigated yet. In addition, though fluorine anion (F^-, 1.36Å)[27] and hydrogen anion (H^-, 1.37Å)[28] have the similar ion radii and the same valence of -1, metal fluorides usually show superior performance to the same metal hydrides as additive. For instance, TiF_3 exhibited superior catalytic effects over TiH_2 on the dehydrogenation of MgH_2[29] or $NaBH_4$.[9] In an effort to understand the significant enhancement in additive activity arising upon variation of the anions, combined phase analyses, microstructure characterization and chemical state analyses were performed on the $NaBH_4$-based composites with REH_2 (RE = rare earth metal) and REF_3 as additives since RE metals could form stable borides,[30] which play an important role in the regeneration of $NaBH_4$. It has been established that the regeneration of borohydrides from metal borides is much easier than that from boron, as the activation energy needed to break the B-M bond is significantly lower than that needed for the B-B bond.[31]

In the present study, a comparison study is carried out both experimentally and theoretically to elucidate the promoting effects of two Lanthanum compounds, LaH_2 and LaF_3, on the hydrogen sorption thermodynamic and kinetic properties of $NaBH_4$. The de-/rehydrogenation mechanisms and nucleation mechanisms have been discussed in detail, as well as the function of F^- and La^{3+} in the de-/rehydrogenation processes of $NaBH_4$. In particular, the re-/dehydriding cyclic behaviors of the two $NaBH_4$ based composites were investigated with the purpose to study the effect of cycling on operating temperatures, de-/rehydrogenation kinetics, and hydrogen capacity. The coupled experimental and theoretical studies may provide a new promising approach for simultaneously improving the thermodynamic and kinetic properties of $NaBH_4$ by combining functional effects of anions and cations.

2. Experimental

Commercial pure La (99%) powders were purchased from Aladdin Reagent Database, Inc. $NaBH_4$ (98%) and LaF_3 (99.9%) were obtained from Strem Chemicals Inc. and Alfa Aesar, respectively. All of these materials were used as received states without any treatments. The sample storage and handling were performed in a Lab 2000 glove box (Etelux Intertgas system Co., Ltd.) filled with purified argon. The $3NaBH_4/LaF_3$ mixture was prepared by mechanical ball milling under Ar atmosphere for 16 h using a QM-1SP2 planetary ball mill at 456 rpm in a stainless steel vessel. For the sake of comparison, two grams of $NaBH_4$ and La powders also in a 3:1 molar ratio were milled under the same conditions. The stainless steel vessel for ball milling was 100 ml, and the weight ratio of the sample to the ball was 1:30.

The hydriding/dehydriding properties were measured in a Sievert type pressure-composition-temperature (PCT) apparatus manufactured by Shanghai Institute of Microsystem and Information Technology. The PCT measurements were performed at different temperatures in the hydrogen pressure range of 0.0019 ~ 4.6 MPa. Pressure of the samples were automatically monitored and recorded. For the isothermal dehydrogenation kinetic measurement, the sample chamber was firstly filled with 5 MPa hydrogen, then after the temperature being quickly raised to and kept at the desired one, the sample chamber was quickly evacuated. For hydrogen absorption measurement, an initial H_2 pressure of 3.2 MPa was applied to the dehydrogenated sample for 8 h at 420 ^oC. After 6 dehydrogenation cycles, the 6th hydrogen absorption conditions for $NaBH_4+LaF_3$ and $NaBH_4+LaH_2$ samples were set at 238 ^oC in 6 h and 326 ^oC in 4.3 h under 4.1 MPa hydrogen pressure, respectively. Temperature-programmed-dehydrogenation (TPD) measurements were carried out starting from vacuum with the temperature increased from 25 ^oC to about 480 ^oC ~ 500 ^oC at a heating rate of 2 ^oC min^{-1}. Approximately ~ 3.0g of sample was used for PCT measurements, 150 mg for isothermal de-/rehydrogenation kinetic measurements, and 100 mg for TPD measurements.

Thermogravimetry (TG) and differential scanning calorimetry (DSC) analyses for the two systems were carried out using synchronous thermal analyses (TG/DSC, Netzsch, STA 449 F3 Jupiter). The heating rate was set at 2, 5 and 10 K min^{-1} under 1 bar flowing argon atmosphere with the temperature rising from 26 to 500 ^oC for $NaBH_4+LaF_3$ and 600 ^oC for $NaBH_4+LaH_2$, respectively. About 10 mg of sample was used each time.

The samples at different states were characterized by X-ray diffraction (XRD Rigaku D/MAX-2500, VL/PCX, Cu Kα radiation) from 10° to 90°(2θ) with a step width of 0.02°, X-ray photoelectron spectroscopy (XPS, A AXIS ULTRADLD, Al Kα radiation), Fourier transform infrared spectrometer (FTIR Spectrum 100 facility, Perkin Elmer, Inc., USA). To avoid oxidation during the XRD measurements, samples were flattened into a homemade container in the Ar filled glove box. For the XPS measurements, binding energy calibration of all samples were done using the C 1s peak (284.5 eV), and the Ar^+ ion gun was used for etching. The binding energy spectra were fitted by XPSPEAK software. Vibration spectra of the species in absorbance mode with wavenumbers ranging from 400 to 4000 cm^{-1} were obtained using a KBr tablet method with the mass ratio of the sample to KBr being 1:60 in FITR measurements.

3. Results and discussions

3.1 Thermodynamic calculations on the $NaBH_4$+LaF_3 and $NaBH_4$+LaH_2 systems.

Thermodynamic parameters, for instance, Gibbs free energies (as a function of temperature at 1 atm H_2 pressure) which are evaluated using the HSC Chemistry program,[32] are used to design and predict the $NaBH_4$-based reversible hydrogen storage systems.

For pure $NaBH_4$, the decomposition reaction can be described as:

$$NaBH_4 = NaH + B + 1.5H_2\,(g) \quad (1),$$

for which calculation gives the Gibbs free energy change ΔG = 0 kJ mol^{-1} at 666.5 °C.

For the $NaBH_4$+LaF_3 system, it is expected that the following reaction may occur according to our previous investigations:[6, 7]

$$3NaBH_4 + LaF_3 = 3NaF + 0.5LaB_6 + 0.5LaH_2 + 5.5H_2(g) \quad (2),$$

The equilibrium reaction temperature is calculated to be 468.5 °C when ΔG =0 kJ mol^{-1}.

For the $NaBH_4$+LaH_2 system, the following reactions may take place:

$$6NaBH_4 + LaH_2 = 6NaH + LaB_6 + 10H_2\,(g) \quad (3),$$

$$4NaBH_4 + LaH_2 = 4NaH + LaB_4 + 7H_2(g) \quad (4),$$

and their equilibrium reaction temperatures are 649.8 °C and 649.4 °C, respectively, when ΔG = 0 kJ mol^{-1}. Because of the lack of thermodynamic data for LaB_4 in the HSC Chemistry program, the standard formation enthalpy of LaB_4 was taken from lit.[30]

At 25 °C, the Gibbs free energies of following reactions:

$$0.6NaBH_4 + La = 0.6NaH + 0.1LaB_6 + 0.9LaH_2 \quad (5),$$

$$4/7\ NaBH_4 + La = 4/7\ NaH + 1/7\ LaB_4 + 6/7\ LaH_2 \quad (6),$$

are -98.7 and -99.0 kJ mol^{-1}, respectively. It means that LaH_2 can be obtained by mixing $NaBH_4$ with La at ambient temperature. Indeed, LaH_2 was detected by XRD analysis of the ball milled $NaBH_4$+La mixture, as seen in Fig. 7. The above theoretical analyses indicate that both LaH_2 and LaF_3 show positive effects on destabilization of $NaBH_4$, while LaF_3 displays superior effect over LaH_2.

3.2 Experimental investigations on thermodynamics of the $NaBH_4$+LaF_3 and $NaBH_4$+LaH_2 systems.

It is known that the dehydrogenation temperature is related to the thermal stability of the hydrogen storage material. $NaBH_4$+LaF_3 composite was subjected to PCT measurements for the characterization of thermodynamic properties. The de-/absorption enthalpy and entropy changes are calculated using van't Hoff equation, and are expressed as follows: Ln (P_{eq}) = - $\Delta H/RT + \Delta S/R$, where P_{eq} is the equilibrium reaction pressure, T the absolute temperature, and R the gas constant. Fig. 1(a) and 1(b) show the PCT curves of the $NaBH_4$+LaF_3 composite at 385, 404, 415 and 425 °C and corresponding van't Hoff plots, respectively. The van't Hoff equations derived from Fig. 1 are expressed as Ln (P_{eq} / MPa) = - 8.72 / T + 12.45 for desorption and Ln (P_{eq} / MPa) = - 3.82 / T + 6.52 for absorption. The corresponding desorption enthalpy and entropy changes are therefore calculated to be 72.5 kJ mol^{-1} H_2 and 103.5 J K^{-1} mol^{-1} respectively; and the absorption enthalpy and entropy changes are -31.8 kJ mol^{-1} H_2 and 54.2 J K^{-1} mol^{-1}, respectively. The obtained

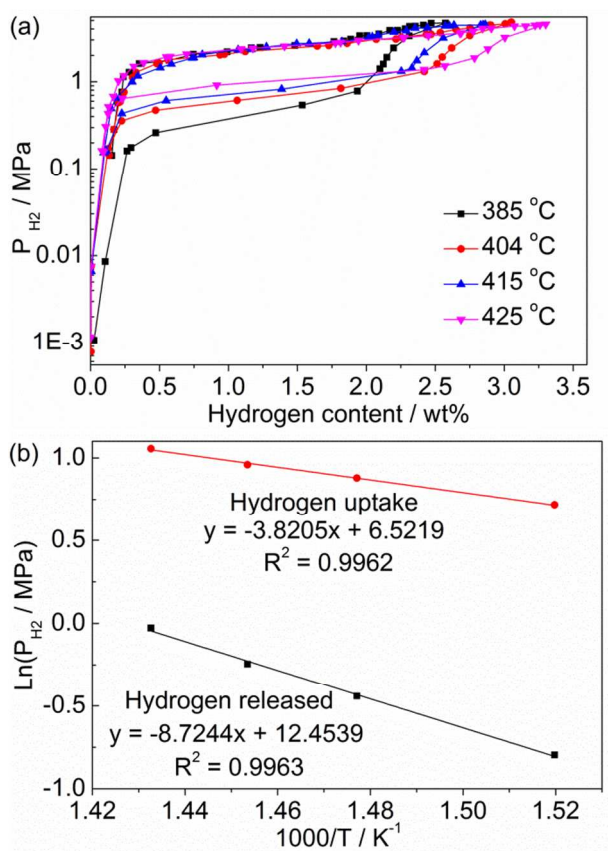

Fig. 1 PCT curves (a) of the $NaBH_4$+LaF_3 composite at various temperatures and the corresponding van't Hoff plots (b).

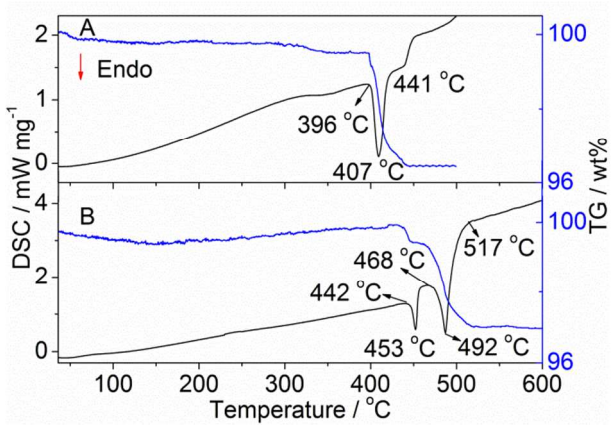

Fig. 2 DSC/TG curves of $NaBH_4$+LaF_3 (A) and $NaBH_4$+LaH_2 (B) samples measured at a heating rate of 2 K min^{-1} under 1 atm argon atmosphere.

desorption enthalpy is reduced by 28 % relative to that of the pure $NaBH_4$ (100 kJ mol^{-1} H_2),[11] which accounts for the decreased dehydrogenation temperature in the $NaBH_4$+LaF_3 system. Because of the sluggish absorption kinetic in the $NaBH_4$+LaH_2 system, equilibrium absorption and desorption reactions are not achieved in PCT measurements of the $NaBH_4$+LaH_2 system, thus the de-/absorption enthalpy and entropy changes cannot be obtained. Nevertheless, DSC analyses given in Fig. 2 will show that the de-/absorption enthalpies of $NaBH_4$+LaH_2 lie between those of $NaBH_4$+LaF_3 and pristine $NaBH_4$.

As seen in Figs. 7 and 8, NaF, LaB_6 and LaH_2 were obtained in the dehydrogenated $NaBH_4$+LaF_3 sample, and NaH and LaB_4 were present in $NaBH_4$+LaH_2 sample. Therefore, it is anticipated that the dehydrogenation follows the stoichiometric reaction (2) in $NaBH_4$+LaF_3 system and (4) in $NaBH_4$+LaH_2 system. Therefore, calculated by HSC Chemistry program, the desorption enthalpy of $NaBH_4$+LaF_3 is 71 kJ mol^{-1} H_2, which is slightly different from the value obtained by PCT measurements. The desorption enthalpy of $NaBH_4$+LaH_2 is calculated to be 92 kJ mol^{-1} H_2, which is also lower than that of pure $NaBH_4$. The formation of LaB_6 or LaB_4 in dehydrogenation products of $NaBH_4$ based composite systems instead of B should contribute to the reduction in desorption enthalpy of $NaBH_4$. On the other hand, the different reactivity of LaF_3 and LaH_2 toward $NaBH_4$ could be understood from the thermochemical point of view.

3.3 A comparative study of dehydrogenation behaviors in $NaBH_4$+LaF_3 and $NaBH_4$+LaH_2 systems.

The effect of the LaF_3 and LaH_2 on lowering the hydrogen desorption temperature of $NaBH_4$ was evaluated by DSC/TG measurements on $NaBH_4$+LaF_3 and $NaBH_4$+LaH_2 systems, as shown in Fig. 2. The endothermic peaks on DSC curves together with mass loss on TG curves correspond to the hydrogen desorption of each composite, and position represents the temperature at which the maximum dehydrogenation rate of each reaction is achieved. There are differences between the two systems and pure $NaBH_4$ at the onset dehydrogenation temperatures in the DSC profiles. For the ball-milled samples, the dehydrogenation starts at 396 °C for the $NaBH_4$+LaF_3 system and 442 °C for the $NaBH_4$+LaH_2 system, respectively. Both of the two temperatures are lower than that of pure $NaBH_4$ (517 °C) measured under the same condition.[8] Indeed, for the $NaBH_4$+LaF_3 system, the DSC signal is composed of a strong endothermic peak at 407 °C, and a shoulder at around 441 °C. In contrast, one small sharp peak at 453 °C and a subsequent sharp peak at 492 °C are recorded for the $NaBH_4$+LaH_2 system. Moreover, the dehydrogenation is complete at 517 °C in the $NaBH_4$+LaH_2 system. It has been shown that the melting temperature of $NaBH_4$ is 505 °C, which is higher than the values recorded for the endothermic peaks of the $NaBH_4$+LaF_3 system, but lies in the temperature range (468 – 517 °C) of the second endothermic peak in the $NaBH_4$+LaH_2 system, indicating that all the dehydrogenation processes of $NaBH_4$ take place in solid state in the former system, while desorption in liquid $NaBH_4$ may occur in the later system.

For the $NaBH_4$+LaF_3 system, the two endothermic peaks appeared on the DSC curve indicate that two different reactions may take place during dehydrogenation. The dehydrogenation mechanisms of the two systems will be proposed in the following section. The hydrogen released from $NaBH_4$+LaF_3 system is 3.53 wt% in total which is close to its theoretical value (3.56 wt%), indicating a complete dehydrogenation. However, the hydrogen released from the $NaBH_4$+LaH_2 system is 3.03 wt% until temperature reaches 600 °C, which is about 88.6 % of its theoretical value (3.42 wt%). On the other hand, on the basis of

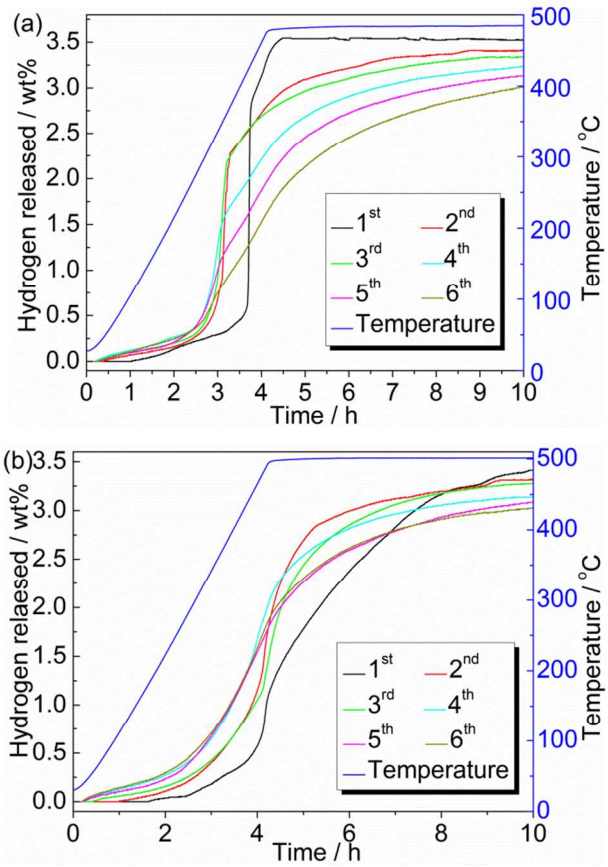

Fig. 3 TPD curves of $NaBH_4$+LaF_3 (a) and $NaBH_4$+LaH_2 (b) samples as a function of temperature measured at a heating rate of 2 K min^{-1} for all cases.

the DSC/TG results shown in $NaBH_4$+LaH_2 system, the enthalpy change of the dehydrogenation reaction, corresponding to the first endothermic desorption peak, is calculated to be 89.6 kJ mol^{-1} H_2, agreeing reasonably with the value obtained by HSC Chemistry program, and also shows a pronounced decreasing in dehydrogenation enthalpy value compared with pure $NaBH_4$. The results obtained from Fig. 2 further indicate that both LaF_3 and LaH_2 are effective in lowering the dehydrogenation temperature of $NaBH_4$, especially a better destabilization effect of LaF_3 with respect to LaH_2.

TPD measurements were used to provide an overall picture of the dehydrogenation process over a wide temperature range and study the reversibility upon cycling of the $NaBH_4$+LaF_3 and $NaBH_4$+LaH_2 systems, as shown in Fig. 3. In the case of the 1st dehydrogenation, the results show that the onset dehydrogenation temperatures are 160 °C and 330 °C for $NaBH_4$+LaF_3 and $NaBH_4$+LaH_2 systems, respectively. In addition, it is seen that the $NaBH_4$+LaF_3 and $NaBH_4$+LaH_2 systems release about 3.5 wt% and 1.2 wt% of hydrogen when temperature reaches 480 °C. After 12 min at 480°C, the dehydrogenation of $NaBH_4$+LaF_3 is complete, with a total hydrogen release of 3.54 wt%. Though the dehydrogenation kinetics of the $NaBH_4$+LaH_2 system is slow, the total amount of released hydrogen is about 3.41 wt% after 10 h. Compared with pure $NaBH_4$ of which the weight loss is only 0.68 wt% after heated at 482 °C for about 14 h,[6] those findings further clearly show that the addition of either LaF_3 or LaH_2 to $NaBH_4$ can enhance the hydrogen desorption rate and increase the weight of hydrogen released from the $NaBH_4$. LaF_3 shows better destabilization effect on the desorption of $NaBH_4$ when compared to LaH_2. Interestingly, a two-step dehydrogenation is observed in case of the $NaBH_4$+LaF_3 system, agreeing well with the result shown in Fig. 2. The 1st step dehydrogenation is in the temperature range from 375 - 423 °C (Fig. 3(a)), while the 2nd step dehydrogenation starts at around 424 °C. Fig. 3(b) shows that the $NaBH_4$+LaH_2 system releases about 0.5 wt% of hydrogen in the temperature range of 30 ~ 468 °C in the 1st dehydrogenation cycle, which is close to the data obtained from DSC/TG measurements, as shown in Fig. 2.

For the $NaBH_4$+LaF_3 system, Fig. 3(a) shows that the amount of hydrogen released from the rehydrogenated sample varies from 3.41 wt% for the 2nd cycle to 3.02 wt% for the 6th cycle. More interestingly, the significant kinetic improvement for desorption is achieved by cycling, that is, the desorption temperature is gradually lowered down by cycling. For example, the maximum desorption rate for the 1st, 2nd, 3rd, 4th, 5th and 6th dehydrogenation is achieved at 407, 333, 319, 306, 295, 282°C, respectively. It implies that some activation processes may occur during the first cycle and show stronger effects with increasing the number of cycles. In the $NaBH_4$+LaH_2 system, Fig. 3(b) displays that hydrogen releases of 3.31wt%, 3.27 wt%, 3.14 wt%, 3.09 wt% and 3.02 wt% are obtained for the 2nd, 3rd, 4th, 5th and 6th cycle, respectively. The decrease in dehydrogenation temperature along with cycling number is also observed. In addition, the slope of the 1st desorption curve is different from the following cycles of which curves are parallel to each other. This means that the cycling not only decreases the dehydrogenation temperature, but also remarkably improves the dehydrogenation rate. For example, when heated for 5 h, the $NaBH_4$+LaH_2 system releases about 1.75 wt% hydrogen in the 1st cycle, while in the 2nd, 3rd , 4th , 5th and 6th cycle, about 2.72, 2.50, 2.60, 2.25 and 2.3 wt% hydrogen can be released, respectively. These results display a good cycling performance in both $NaBH_4$+LaF_3 and $NaBH_4$+LaH_2 systems accompanied with a slight drop in hydrogen sorption capacity over 6 cycles. The similar phenomenon has been seen in the $LiBH_4$-base and $NaBH_4$-based hydrogen storage systems upon cycling.[6, 33-38] Moreover, the TPD results indicate that $NaBH_4$+LaF_3 system shows superior dehydriding kinetic upon cycling, whereas $NaBH_4$+LaH_2 system shows a lower capacity drop over 6 cycles (0.51 wt% for $NaBH_4$+LaF_3 system; 0.38 wt% for $NaBH_4$+LaH_2 system).

In both cases, the observed decomposition temperature is lower than the theoretically predicted one as calculated by HSC

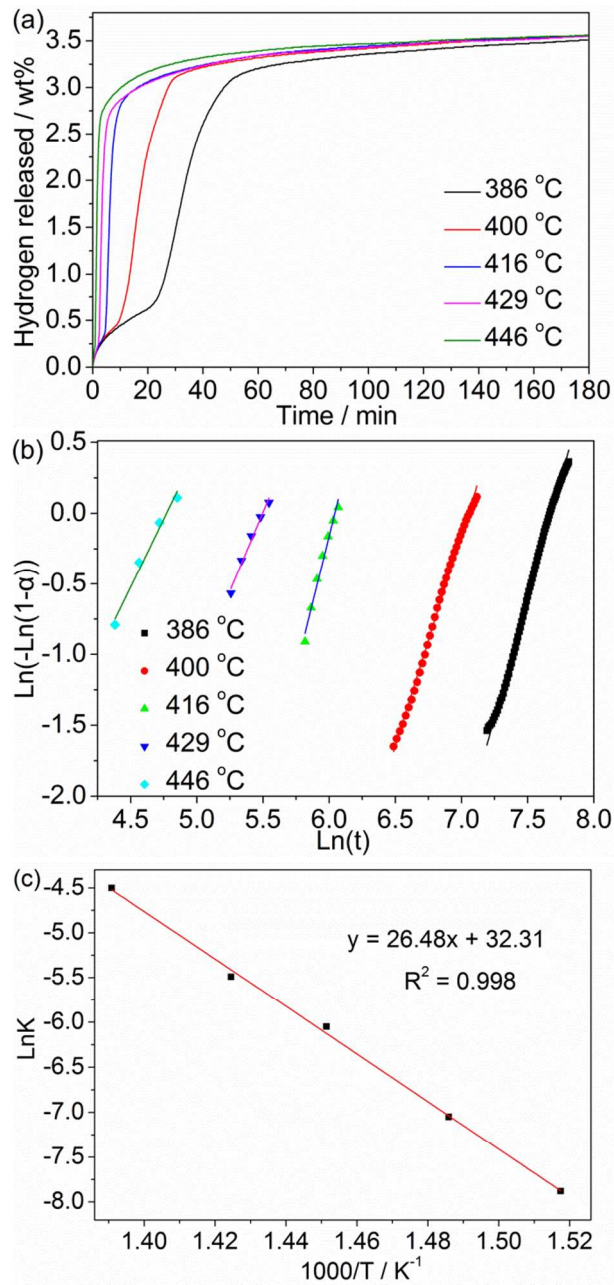

Fig. 4 Isothermal dehydrogenation curves (a) of $NaBH_4$+LaF_3 measured at 386-446 °C, the corresponding JMA plot (b) and Arrhenius plot (c).

Chemistry program, which may result from the different reaction pathways between theoretical depicted one and the real one. In particular, the applied recharging conditions (420 °C, 3.2 MPa hydrogen) in the present study is more favorable compared with those applied for $NaBH_4$ with metal or metal hydride/halide/oxides additives (450-500 °C, 5.5-6MPa).[9, 22]

3.4 A comparative study of de-/absorption kinetics in $NaBH_4$+LaF_3 and $NaBH_4$+LaH_2 systems.

The time dependent kinetic behaviors for isothermal solid-state reaction was usually described by Johanson-Mehl-Avrami (JMA) equation.[39, 40] To elucidate the dehydrogenation kinetic modes, the $NaBH_4$+LaF_3 and $NaBH_4$+LaH_2 systems were subjected to

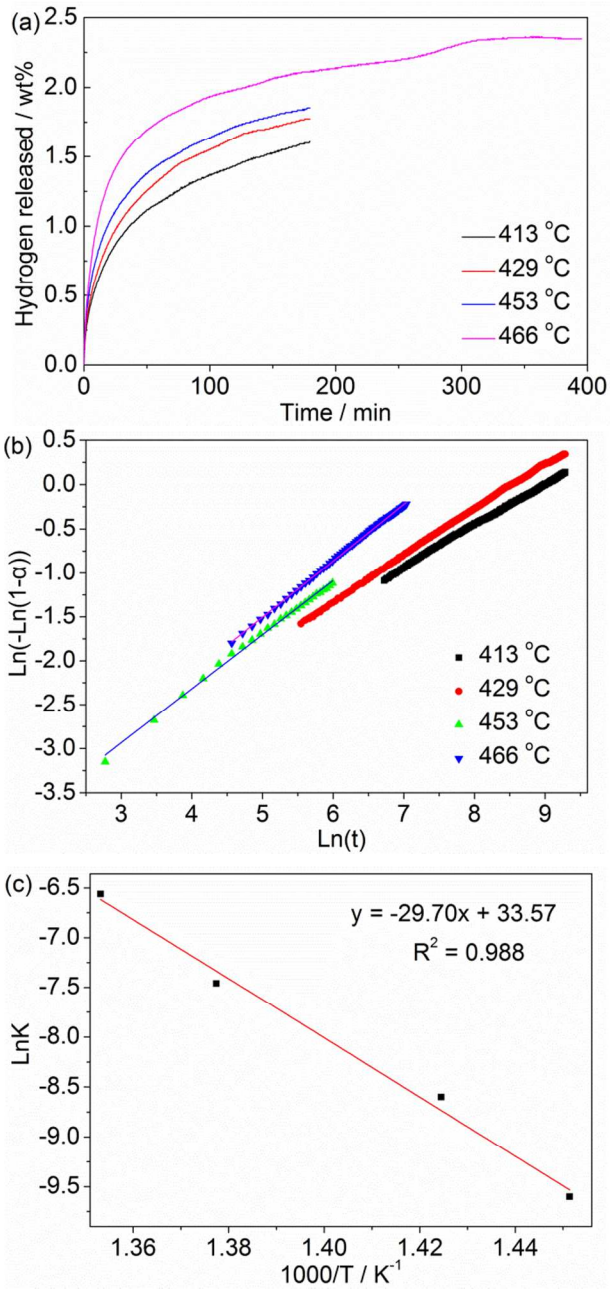

Fig. 5 Isothermal dehydrogenation curves (a) of $NaBH_4$+LaH_2 measured at 413-466 °C, the corresponding JMA plot (b) and Arrhenius plot (c).

the isothermal dehydrogenation measurements at different temperatures, and the behaviors were described in the framework of the JMA model presented below:[41]

$$\alpha(t) = 1 - \exp[-(kt)^n] \qquad (7),$$

where $\alpha(t)$ was the fraction given as function of time t, k the temperature-dependent kinetic constant, and n the Avrami exponent related to the transformation mechanism. Fig. 4(a) and 5(a) show the isothermal dehydrogenation curves of the $NaBH_4$+LaF_3 and $NaBH_4$+LaH_2 systems at different temperatures. As expected, dehydrogenation is dramatically accelerated as the temperature increases, especially in the $NaBH_4$+LaF_3 system. For example, a dehydrogenation capacity of 2.8 wt% is achieved in 44 min at 386 °C, while the same amount can be reached within 4 min at 446 °C. Additionally, the total hydrogen desorption capacity is about 3.53 wt% in the temperature range 386 - 446 °C, which is close to the theoretical value (3.56 wt%), demonstrating a complete dehydrogenation in $NaBH_4$+LaF_3 system. In contrast, about 1.19, 1.36, 1.47 and 1.78 wt% of hydrogen can be released from the $NaBH_4$+LaH_2 system at 413, 429, 453 and 466 °C in 60 min, and 1.59, 1.77, 1.85 and 2.12 wt% in 180 min, respectively. Furthermore, the system can desorb 2.37 wt% hydrogen after 400 min at 466 °C. According to lit.,[6] only 0.212 wt% hydrogen is released from pure $NaBH_4$ after being heated at 400 °C for 1 h. Therefore, Fig. 4(a) and 5(a) show that both LaH_2 and LaF_3 could improve the dehydrogenation kinetics of $NaBH_4$ to different degrees. It is believed that the dehydrogenation rate is correlated to the nucleation of the products in the dehydrogenation process.[23, 42] A linear interpolation of the typical master plots, $\ln(-\ln(1-\alpha))$ vs $\ln(t)$ in the range $0.15 \le \alpha \le 0.85$, yields the values of n and k given in table 1, which could be used to shed light on the dehydrogenation modes in $NaBH_4$+LaF_3 and $NaBH_4$+LaH_2 systems. The results were displayed in Fig. 4(b) and Fig. 5(b). For the $NaBH_4$+LaF_3 system, the Avrami exponent n obtained is in the range from 1.93 to 3.77, corresponding to a diffusion controlled reaction mechanism, and nucleation should be of early nucleation-site saturation.[43] In addition, it is shown that the value of n is somewhat temperature dependent. Furthermore, the Avrami exponent n is around 3 - 4 in the temperature range 386 - 416 °C, indicating that the main nucleation occurs at the grain corners.[43] At 429 - 446 °C, the value of n is in the range 1.93 - 2.22, implying that the new phase nucleation belongs to the decreasing nucleation rate mode. In contrast, in the $NaBH_4$+LaH_2 system, the value of n is in the range from 0.45 to 0.70 within the experiment temperatures from 413 to 466 °C, suggesting a random nucleation mechanism with early nucleation at dislocations or highly anisotropic of growth velocities.[44] It is known that random nucleation impedes ion transportation.[44] Therefore, such a nucleation and growth mechanism might lead to the incubation period in $NaBH_4$+LaH_2 system shown in Fig. 2, for which desorption stops for a limited time (about 3 min) in the range 460 - 470 °C. As the temperature increases, especially close to the melting point of $NaBH_4$, since the rate of ion transportation is accelerated, the hydrogen desorption proceeds again until the decomposition was complete. The similar phenomenon has been observed in $Ca(BH_4)_2$ and $LiBH_4$-MgH_2 systems.[45, 46]

For dehydrogenation, the $NaBH_4$+LaF_3 system shows faster dehydriding kinetics over the $NaBH_4$+LaH_2 system. The

difference may be ascribed to the substitution of F^- for H^-, since F^- and H^- have the similar ionic radii. The similar phenomenon has also been reported in metal fluoride doped metal borohydride systems.[6, 47] On the other hand, in the study of metal hydride-Alkali metal borohydride systems, desorption occurred after the melting of Alkali metal borohydrides.[22, 48] As seen from DSC curves in Fig. 2, the highest dehydrogenation rate is achieved at 491 °C, which is also close to the melting point of $NaBH_4$, indicating that the rapid dehydrogenation takes place when $NaBH_4$ is partially melted. In the isothermal dehydrogenation measurements, when the temperature is in the range from 413 to 466 °C (lower than the melting point of $NaBH_4$), the dehydrogenation in the $NaBH_4$+LaH_2 system suffers from a slow diffusion rate compared with that in the liquid state. The above factors account for the change in the value of n, and as a consequence, result in the different dehydrogenation rates between $NaBH_4$+LaF_3 and $NaBH_4$+LaH_2 systems.

Arrhenius equation is used to determine the apparent activation energy E_a of dehydrogenation reaction for the two systems by executing the exponential fitting. The temperature-dependent reaction rate k reflects the nucleation rate and the growth rate of the dehydrogenation process and could be described by Arrhenius formulation: $k = k_o \exp(-\frac{Ea}{RT})$, where k_o is the pre-exponential factor. The plot of Lnk against 1000/T, which exhibits a good linearity, is shown in Fig. 4(c) and Fig. 5(c). The values of E_a obtained from the slope of the plots for $NaBH_4$+LaF_3 and $NaBH_4$+LaH_2 systems are 220.1 and 247.0 kJ mol^{-1}, respectively. The results demonstrate that the energy barrier needed to be overcome in dehydrogenation process of the $NaBH_4$+LaF_3 system is lower than that in the $NaBH_4$+LaH_2 system. Additionally, the reaction rate constants for $NaBH_4$+LaF_3 and $NaBH_4$+LaH_2 systems are calculated to be $k = 50\times10^{-4}$ s^{-1} and $k = 1.5\times10^{-4}$ s^{-1} at the given temperature of 430 °C, respectively, which agree well with the fact that the dehydrogenation kinetics in $NaBH_4$+LaF_3 is much faster than that in the $NaBH_4$+LaH_2 system.

Table 1 Data for the dehydrogenation kinetics of $NaBH_4$+LaF_3 and $NaBH_4$+LaH_2 systems

sample	T/°C	n	-LnK	K($\times10^{-4}$ s^{-1})
$NaBH_4$+LaF_3	386	3.30	7.88	3.78
	400	2.98	7.05	8.67
	416	3.77	6.05	23.58
	429	2.22	5.49	41.28
	446	1.93	4.50	111.1
$NaBH_4$+LaH_2	413	0.45	9.60	0.68
	429	0.50	8.60	1.84
	453	0.63	7.46	5.76
	466	0.70	6.57	14.02

The function of LaH_2 and LaF_3 on the rehydrogenation of $NaBH_4$ was further investigated by isothermal hydrogenation measurements as shown in Fig. 6. It is seen that hydrogenation performances of $NaBH_4$ are significantly improved by both LaH_2 and LaF_3. Clearly, about 3.33 wt% and 3.46 wt% hydrogen were absorbed at 420 °C under 3.2 MPa hydrogen pressure in $NaBH_4$+LaH_2 and $NaBH_4$+LaF_3 systems, respectively, while the regeneration of $NaBH_4$ from its decomposition products

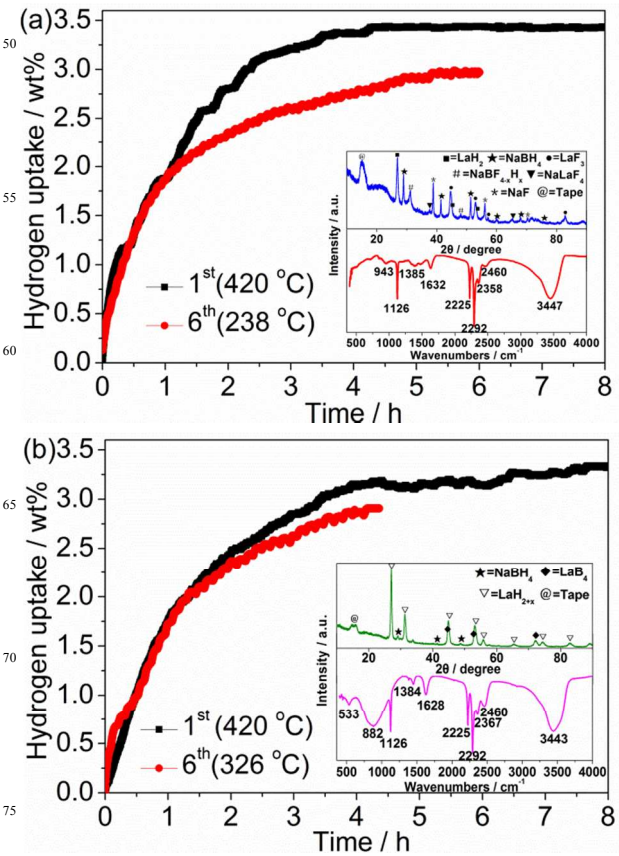

Fig. 6 Isothermal rehydrogenation curves of (a) $NaBH_4$+LaF_3 for the 1st time (420 °C, 3.2MPa H_2) and the 6th time (238 °C, 4.1 MPa H_2); (b) $NaBH_4$+LaH_2 for the 1st time (420 °C, 3.2MPa H_2) and the 6th time (326 °C,4.1 MPa H_2). The insets show the XRD and FTIR patterns of the 6th rehydrogenation products of $NaBH_4$+LaF_3 and $NaBH_4$+LaH_2 systems.

(NaH+B) under 400 °C and 350 bar hydrogen pressure for 24 h was unsuccessful.[49] The results indicate that the activation energy needed for the reconstruction of $[BH_4]^-$ ligand is much lower in the dehydrogenated products of the two composites than that in the dehydrogenated pure $NaBH_4$. In addition, La-B phases and LaH_2 appeared in the dehydrogenation products of both $NaBH_4$+LaF_3 and $NaBH_4$+LaH_2 systems. Therefore, Fig. 6 shows similar isothermal hydrogenation curves for the two composites, though LaH_2 has different effects on the hydrogenation process in the two systems. On the other hand, there exists the difference, such as NaF and NaH in the dehydrogenation products of $NaBH_4$+LaF_3 and $NaBH_4$+LaH_2 systems, respectively. NaF makes the hydrogen absorption kinetics to be faster in the former system over the later one. The reason could be raised from the appearance of thermodynamically more stable compound in the rehydrogenated sample of $NaBH_4$+LaF_3 system (eg. LaF_3, of which $\Delta_f H$ is -1699.541 kJ mol^{-1}) than in that of $NaBH_4$+LaH_2 system (eg. LaH_2, of which $\Delta_f H$ is -201.25 kJ mol^{-1}). The differences in hydrogenation kinetic effect caused by F^- containing phase have been observed in the study of hydrogenation in LiF-MgB_2 [47] and LiH-MgB_2 [50] composites.

For the 6th dehydrogenation, temperatures at which the maximum dehydrogenation rates were achieved were lowered

down to 286 and 328 °C for $NaBH_4$+LaF_3 and $NaBH_4$+LaH_2 systems, respectively. Therefore, the 6th dehydrogenation products were subjected to rehydrogenation at 238 and 326 °C under 4.1 MPa hydrogen pressure, as shown in Fig. 6. The results demonstrate that after 6 dehydrogenation cycles, both of the two systems exhibit excellent hydrogenation performance at relatively low temperatures. Hydrogen storage capacities of 3.0 wt% and 2.9 wt% are obtained under 4.1 MPa H_2 in $NaBH_4$+LaF_3 system at 238 °C in 6 h and $NaBH_4$+LaH_2 system at 326 °C in 4.3 h, respectively. Apart from a slight capacity drop, Fig. 6 shows a remarkable improvement in hydrogenation kinetics of $NaBH_4$ and a significant reduction in hydrogenation temperatures for both of the two systems.

XRD and FTIR patterns of the $NaBH_4$+LaF_3 and $NaBH_4$+LaH_2 samples after the 6th rehydrogenation are shown in the inset of Fig. 6. Clearly, $NaBH_4$ and LaF_3 are found in the XRD pattern shown in the inset-up of Fig. 6(a), implying that $NaBH_4$ is regenerated in the $NaBH_4$+LaF_3 sample after the 6th hydrogenation at 238 °C. Moreover, the typical B-H vibration band located at 1126, 2225, 2292, and 2358 cm^{-1} are present in the inset-down of Fig. 6(a), further demonstrating the restoration of $NaBH_4$ at relatively low temperatures. In case of the $NaBH_4$+LaH_2 system, XRD and FTIR patterns shown in the inset of Fig. 6(b) also evidence the regeneration of $NaBH_4$ in the $NaBH_4$+LaH_2 system after the 6th hydrogenation process at 328 °C. These results clearly demonstrate that a significant improvement in absorption kinetics is achieved by cycling. In addition, partially unconverted NaF in the $NaBH_4$+LaF_3 system (seen in Fig. 6(a)) and LaB_4 in the $NaBH_4$+LaH_2 system (seen in Fig. 6(b)), which are resulted from the kinetic delay, might be responsible for the capacity drop during cycling in the two systems. It is known that size reduction of particle can decrease hydrogen diffusion lengths and increase surface interaction areas with H_2. Therefore, the size reduction of nanoparticle can tailor thermodynamic and kinetic properties of hydrogen desorption/absorption in complex metal hydrides.[51, 52] Based on the Scherrer equation, the particle sizes of $NaBH_4$ after ball milling are approximately 45.79 nm and 52.89 nm in $NaBH_4$+LaF_3 and $NaBH_4$+LaH_2 systems, respectively. In contrast, after the 6th rehydrogenation, they reduce to 20.43 nm and 26.70 nm, respectively. The size reduction of $NaBH_4$ particles achieved by cycling accounts for the significant improvement in desorption and absorption kinetics during the 6 cycles in both $NaBH_4$+LaF_3 and $NaBH_4$+LaH_2 systems.

It is reported that the decomposition of $NaBH_4$ in 2$NaBH_4$-MgH_2 system is 509 °C, and rehydrogenation takes place at 450 °C under 6 MPa hydrogen pressure with catalyst doping.[22] In $NaBH_4$-0.05TiH_2 composite, the dehydrogenation of $NaBH_4$ is about 450 °C, and rehydrogenation is performed at 500 °C under 5.5 MPa hydrogen pressure.[9] It is worth noting that the dehydrogenation temperature, the hydrogenation temperature, and hydrogenation pressure are all lower in the $NaBH_4$+LaH_2 system than those in 2$NaBH_4$-MgH_2 and $NaBH_4$-0.05TiH_2 systems, indicating a superior effect of LaH_2 over MgH_2 and TiH_2 on reversible hydrogen sorption in $NaBH_4$. Table 2 summarizes temperatures, hydrogen pressures and time needed for rehydrogenation in some RHC systems. More importantly, as lanthanide elements have similar chemical properties, the finding in this work, that is, LaH_2 can promote the regeneration of $NaBH_4$, may extend to other lanthanide hydrides.

Table 2 Data for hydrogen uptake in MBH_4 (M=Li, Na)-M'H_2 (M'= metal) without or with catalysts

Composite	Rehyd				
	Temp / °C	Pressure / MPa	Time / h	Obs Rehyd H_2 / %	Ref.
$LiBH_4$-TiH_2	400	15	50	Unsuccessful	[53]
$LiBH_4$-ScH_2	400	15	50	Unsuccessful	[53]
$LiBH_4$-CaH_2	400	35	24	Unsuccessful	[49]
$LiBH_4$-CaH_2/$TiCl_3$	450	10	15	90	[54]
$LiBH_4$-MgH_2	400	35	24	95	[49]
$NaBH_4$-MgH_2	400	35	24	89	[49]
$NaBH_4$-MgH_2/TiF_3	600	4	12	75	[55]
$NaBH_4$-CaH_2	400	5.5	10	Unsuccessful	[56]
$LiBH_4$-CaH_2/$TiCl_3$	400	10	20	93	[48]
$LiBH_4$-LaH_2	400	6	4	80	[24]
$LiBH_4$-CeH_2	400	6	4	67	[24]
$NaBH_4$-LaH_2	420(326[a])	3.2(4.1[a])	4.2(4.2[a])	94(85[a])	This work

[a] Data obtained from the 6th rehydrogenation measurement.

3.5 Understanding of the de-/absorption mechanisms and the function of F anion and La cation.

In order to understand the mechanisms of LaH_2 and LaF_3 on the de-/rehydrogenation of $NaBH_4$, the phase and chemical state analyses of $NaBH_4$+LaH_2 and $NaBH_4$+LaF_3 samples were conducted by XRD, FTIR and XPS measurements at various states. In the $NaBH_4$+LaH_2 system, Fig. 7 shows that the strong diffraction peaks of LaH_2 clearly appear in the ball-milled sample, which is in good agreement with the prediction obtained by HSC Chemistry program, proving that the reaction between $NaBH_4$ and La should take place as reaction (6) during ball milling. G. Renaudin reported that the cubic LaH_2 phase was a nonstoichiometric compound having a general formula of LaH_{2+x}, where x varied from 0~1.[57] This LaH_{2+x} phase is slightly left-shifted after being heated to 230 °C, as shown in Fig. 7(a)(A). Until 400 °C, the peaks of LaH_2 and $NaBH_4$ turn to be weak, indicating that $NaBH_4$ has reacted with LaH_2 to release hydrogen, as seen in Fig. 7(a)(B). At 450 °C for 1.5 h, LaB_4 and NaH are present, but weak peaks from $NaBH_4$ still exist, as well as peaks from LaH_2, indicating that the dehydrogenation is incomplete. When the temperature reaches 480 °C, the dehydrogenated sample is composed mostly of LaB_4 and NaH, leaving LaH_2 as surplus due to the unbalanced ratio of $NaBH_4$ to LaH_2. Therefore, the dehydrogenation reaction could be described as reaction (4).

After being rehydrogenated at 420 °C under 3.2 MPa hydrogen for 8 h, diffraction peaks from restored $NaBH_4$, LaH_2 and residual LaB_4 can be detected, as shown in Fig. 7(a)(E). The presence of residual LaB_4 results in the partial reversibility of $NaBH_4$ under

the applied conditions. The hydrogenation reaction can be described as the inverse of the dehydrogenation reaction. The dehydrogenated $NaBH_4$+LaH_2 composite can absorb 3.32 wt% hydrogen in 8 h (97 % of the theoretical value), as shown in Fig. 6(b). The good reversibility without any catalytic additives is remarkably interesting, since most $LiBH_4$ or $NaBH_4$-based reactive hydride composites show the reversibility only with catalytic additives, except in the case of MgH_2 added $LiBH_4$, $NaBH_4$ or $Ca(BH_4)_2$ based composites, for which dehydrogenation products could be rehydrogenated at 20 - 35 MPa hydrogen pressure for 24 h. In addition, x in LaH_{2+x} in the ball-milled and rehydrogenated samples is around 1, and is around 0.05 in the dehydrogenated samples. Neutron diffraction study on the hydrides of LaH_{2+x} has shown that the lattice parameter decreases monotonically as x increases,[57] which could explain the fact that the peaks of LaH_{2+x} in the dehydrogenated samples is slightly left-shifted compared to the corresponding peaks of the hydrogenated and ball-milled ones. Fig. 7(b) shows that 4 peaks from $[BH_4]^-$ ligand appear in the FTIR spectrum of the ball milled sample, 1126 cm^{-1} corresponding to the bending band of B-H, while 2225, 2292 and 2366 cm^{-1} corresponding to the stretching band, which are located in the B-H vibration range of $NaBH_4$, according to lit.[6] Moreover, peaks belonging to $NaBH_4$ turn to be weaker until they disappear as temperature increases in the dehydrogenation process. Meanwhile, the peak corresponding to NaH located at 886 cm^{-1} [9] appears and its intensity increases gradually, which is in good agreement with the result shown in Fig. 7(a). After hydrogenation, the peak intensity of $NaBH_4$ becomes stronger, which further demonstrates the restoration of $NaBH_4$. In addition, a new weak peak around 2500 cm^{-1} is also observed in de-/rehydrogenation products, which may come from trace amount of $Na_2B_{12}H_{12}$, since it is a very stable by-product.[6] Besides the random nucleation mechanism respects to the appearance of incubation period in $NaBH_4$+LaH_2 system before temperature reaches the melting point of $NaBH_4$, another possibility resulting in incubation period in $NaBH_4$+LaH_2 system is the formation of $Na_2B_{12}H_{12}$, which occurs at the surface of the metal hydride,[58] blocking the direct contact between $NaBH_4$ and LaH_2.

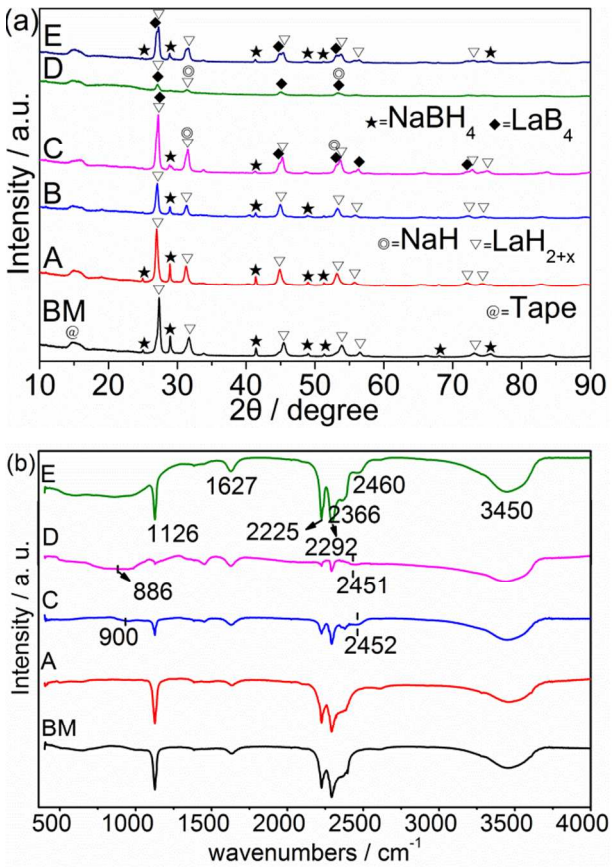

Fig. 7 XRD patterns (a) and FTIR patterns (b) of the $NaBH_4$+LaH_2 composite after ball-milling (BM), the first dehydrogenation at 230 °C (A), 400 °C (B), 450 °C (C), 480 °C (D) and after rehydrogenation (E).

Fig. 8(a) shows that after ball milling, no new phases can be detected in $NaBH_4$+LaF_3 system except $NaBH_4$ and LaF_3, indicating a simple physical mixing of $NaBH_4$ and LaF_3. LaF_3 reacts with $NaBH_4$ at elevate temperatures. The slightly weakened diffraction peaks of $NaBH_4$ and LaF_3 are identified at 220 °C as shown in Fig. 8(a)(A), and the diffraction peaks of $NaBH_4$ disappear when the temperature reaches 430 °C (Fig. 8(a)(B)). Meanwhile, the peaks of NaF, LaB_6, residual LaF_3, as well as La-hydride phases are present. After dehydrogenated at 460 °C, the peak intensity of LaB_6 increases with the appearance of LaB_4. According to reaction (4), the appearance of LaB_4 may

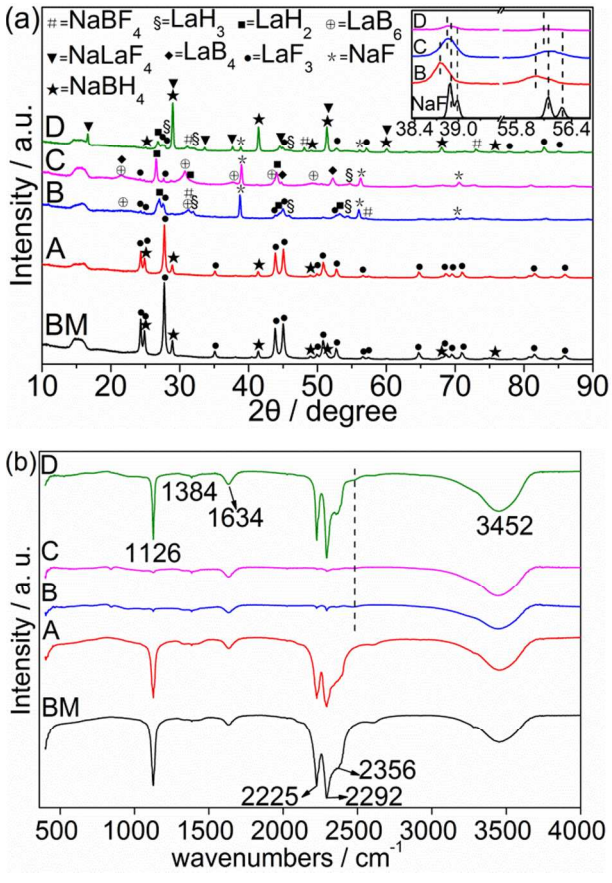

Fig. 8 XRD patterns (a) and FTIR patterns (b) of the $NaBH_4$+LaF_3 composite after ball-milling (BM), the first dehydrogenation at 220 °C (A), 430 °C (B), 460 °C(C) and after rehydrogenation (D). The partial enlarged XRD patterns together with the diffraction pattern of NaF are given inset of Fig. a.

result from the reaction between LaH_2 and $NaBH_4$. Therefore, it can be deduced that there are two reactions at the elevated temperatures during the dehydrogenation process in $NaBH_4$+LaF_3 composite, and can be described as: reaction (2) takes place during dehydrogenation process, if the temperature exceeds 424 ^oC, reaction (4) will occur following reaction (2). On the other hand, reaction (4) taking place in $NaBH_4$+LaF_3 system consumes a portion of $NaBH_4$, which results in residual LaF_3 in the complete dehydrogenated $NaBH_4$+LaF_3 sample, as seen in Fig. 8(a)(C).

The corresponding FTIR results obtained from Fig. 8(b) are consistent with XRD results shown in Fig. 8(a). After dehydrogenation at 430 ^oC, small amount of residual $NaBH_4$ can be detected by FTIR but is absent in the XRD pattern due to its low content. If LaH_2 is formed at the interface between $NaBH_4$ and LaF_3, it might disturb the destabilization reaction by blocking direct contact between $NaBH_4$ and LaF_3, thus, as temperature increases, the reaction between LaH_2 and the residual $NaBH_4$ may occur. After heated to 460 ^oC, the peaks corresponding to $NaBH_4$ disappear completely.

The hydrogenated $NaBH_4$+LaF_3 sample in Fig. 8(a)(D) shows the peaks corresponding to $NaBH_4$ and LaF_3 together with those of residual NaF and La-hydride. Additionally, $NaLaF_4$ also appears due to the radii ratio of Na^+/La^{3+} being 0.93.[59] The phase of $NaREF_4$ presented in the hydrogenated products has been observed when the radii ratio of M^+/R^{3+} (M = alkali, R = rare earth metals) lies between 0.77 and 1.40.[6, 7, 59] The FTIR spectrum of the hydrogenated sample shows four peaks corresponding to the vibration of B-H coming from $NaBH_4$. This further demonstrates the regeneration of $NaBH_4$. The unconspicuous peak of $Na_2B_{12}H_{12}$ indicates that only very small portion of $NaBH_4$ decomposes alone. On the other hand, this result also demonstrates a rapid dehydrogenation reaction between $NaBH_4$ and LaF_3. Based on the XRD and FTIR results, the hydrogenation reactions could be the reverse reaction of (2) accompanied with :

$$NaF+LaF_3=NaLaF_4 \qquad (8).$$

If the dehydrogenation temperature exceeds 424 ^oC, the hydrogenation reaction also includes the reverse reaction of (4). These reactions may take place simultaneously during the rehydrogenation process. It should be noted that the peak located at around 1630 cm^{-1} can be assigned to the bending band of H-O-H, while the peak at 3450 cm^{-1} is the O-H stretching band, as shown in both of the two FTIR spectra (Figs. 7 and 8). It is related to the unavoidable moisture absorption of the samples during the FTIR measurements.

It is worth noting that the dehydrogenation in $NaBH_4$+LaF_3 composite undergoes two reactions when temperature rises above 424 ^oC, which is different from that in $3NaBH_4$-NdF_3 or $3NaBH_4$-PrF_3 composites reported in our previous works.[6, 7] However, the reversibility of $NaBH_4$ can be also achieved under moderate conditions in $NaBH_4$+LaF_3 and $NaBH_4$+LaH_2 composites. In both cases, the formation of La-B phases after dehydrogenation is believed to play the major role for the regeneration of $NaBH_4$, as observed in other $NaBH_4$ based composites.[6, 21]

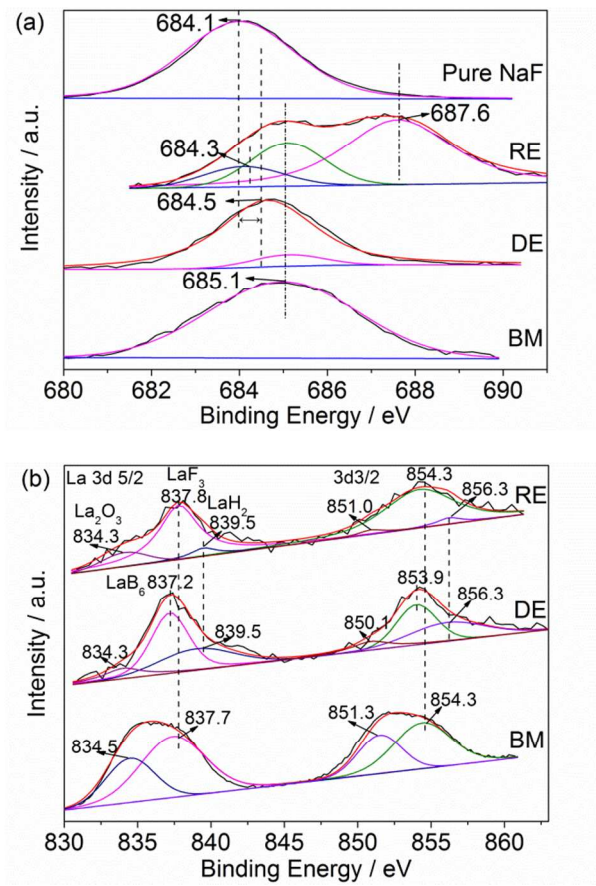

Fig. 9 XPS spectra of F 1s (a) and La 3d (b) in the $NaBH_4$+LaF_3 sample at ball milled and de-/rehydrogenated states, as well as F 1s in pure NaF reference sample for comparison.

LaH_2 and LaF_3 show positive effects on improving de-/rehydrogenation kinetics of $NaBH_4$. The factors contributing to those property improvements of $NaBH_4$ are apparently associated with the F anion and La cation. XPS measurements are used to understand the state and function of the F anion and La cation to further support this speculation in the de-/rehydrogenation of $NaBH_4$+LaF_3 sample.

The state of F anion in the ball milled, dehydrogenated and rehydrogenated samples were examined by XPS measurements, as shown in Fig. 9(a)(BM, DE, RE). Fig. 9(a)(BM) shows that ball milled sample contains F anion having only one chemical state, indicating that only LaF_3 exists in the ball milled sample. According to the XPS result of the NaF reference sample (684.1eV), in the dehydrogenated sample (Fig. 9(a)(DE)), the peak with higher binding energy (684.5eV) should be assigned to the $NaF_{1-x}H_x$ phase, and the peak with binding energy of 681.5 eV comes from the residual LaF_3, coinciding exactly with the XRD result shown in Fig. 8(a)(C). Notably, XPS analysis of the rehydrogenation sample identifies three chemical states of F anion. The first signal appearing at 684.3 eV is assigned to $NaF_{1-x}H_x$ phase, as observed in the dehydrogenated sample. The second one appearing at 685.1 eV is assigned to LaF_3 phase, which demonstrates the recombination of LaF_3 and agrees well with the XRD result of the rehydrogenation sample. The third one with a higher binding energy of 687.6 eV shows a subtle binding energy

shift toward $NaBF_4$ of which peak appears at 687.2 eV.[60] This unknown chemical state may be originated from the substitutional F in the $NaBF_{4-x}H_x$ lattice.

Careful examination of XRD patterns shows that those NaF peaks in $NaBH_4$+LaF_3 samples dehydrogenated at 430 °C, 460 °C (Fig. 8(a)(B) and (C)) and the rehydrogenated sample (Fig. 8(a)(D)) are slightly left-shifted compared to peaks of pure NaF reference sample, as seen in the inset of Fig. 8(a). The peaks at 38.5º - 39.2º and 55.9º - 56.4º correspond to the (200) and (220) peaks of NaF, respectively, which shift slightly toward higher angle side. Such a shift suggests the formation of $NaF_{1-x}H_x$ via a substitution of F^- for H^-, which agrees well with Fig. 9(a)(DE). This phenomenon is not surprising in view of the same crystal structure (cubic) as well as the same space groups (Fm-3m) of NaF and NaH, and has been observed in the mechanically milled NaH-TiF_3 composite.[61] In addition, the new peaks at 2θ of 30.9 - 31.6° in the de-/rehydrogenation products shown in Fig. 8 (a)(B) and (D) correspond to $NaBF_4$, but show smaller lattice parameters, which hint the formation of $NaBF_{4-x}H_x$, also due to the substitution of F^- for H^- in $NaBH_4$ lattice during the de-/rehydrogenation processes. A similar phenomenon has been reported in the previous work.[6] Moreover, the formation of $NaBF_{4-x}H_x$ phase in the rehydrogenated and incomplete dehydrogenated samples is consistent with Fig. 9(a), which could be another support to this assignment. According to the first-principles calculations, partial substitution of F^- for H^- in $LiBH_4$ could result in a favorable thermodynamic modification and thereby lower down the dehydrogenation temperature.[19] To support this assignment, TPD measurements of the rehydrogenated $NaBH_4$+LaF_3 sample were conducted. As shown in Fig. 3, during the 2nd dehydrogenation, the onset dehydriding temperature is as low as 60 °C, which is 100 °C lower than that of the ball milled one. Therefore, the lower onset dehydrogenation temperature should likely be originated from the compositional change arising upon F^- substitution for H^-. The formation of partially F^- substituted complex hydrides, such as $LiBH_{4-x}F_x$ and $Na_3AlH_{6-x}F_x$ phases, has been confirmed in Li-Mg-B-H-F and Na-Al-H-F systems.[16, 17, 47] On the other hand, in case of the reaction between LaH_2 and $NaBH_4$, the temperature needed in $NaBH_4$+LaF_3 system is 12 °C lower than that needed in $NaBH_4$+LaH_2 system, which may also be due to the formation of $NaBF_{4-x}H_x$ having more favorable thermodynamic property than pristine $NaBH_4$, as well as the early formation of LaB_6 which may act as catalyst.

Fig. 9(b) shows the chemical state of La in the ball milled, dehydrogenated and rehydrogenated $NaBH_4$+LaF_3 samples also measured by XPS apparatus. For the ball-milled sample, peak fitting reveals that the La 3d spectrum can be resolved into two sets of $2p_{5/2}$-$2p_{3/2}$ spin-orbit doublets at 834.5 and 837.7eV, and 851.3 and 854.3 eV. The lower binding energy contribution (834.5 eV) is the characteristic of La_2O_3, which is formed due to the oxidation occurred when the sample is taken out from the glove box and loaded to the XPS facility, whereas the second one (837.7 eV) can be attributed to LaF_3 according to lit.[60] After dehydrogenation, the banding energy of La 3d has changed. It is resolved into three sets of $2p_{5/2}$-$2p_{3/2}$ spin-orbit doublets: 834.3-850.1 eV attributed to La_2O_3; 837.2-853.9 eV attributed to LaB_6; 839.5-856.3 eV attributed to LaH_2,[60] which further demonstrates the formation of LaB_6 and LaH_2 in the dehydrogenated sample. In the rehydrogenated sample, it is obvious to see the regenerated LaF_3 as well as the residual LaH_2, which agrees well with the result of Fig. 8(a). Additionally, the binding energy of LaH_2 shifts slightly toward higher value compared with that given in lit.[60] of which banding energy is in the range from 838.5 to 839.0 eV for La $3d_{5/2}$, and it might also result from the substitutional F in the LaH lattice. LaB_6 appeared in the dehydrogenated sample will act as the active center to allow the regeneration of $NaBH_4$ during rehydrogenation process.[31] It is therefore believed that both La^{3+} and F^- play important roles in the de-/rehydrogenation processes of the $NaBH_4$+LaF_3 system. In both $NaBH_4$+LaH_2 and $NaBH_4$+LaF_3 systems, a series of experimental evidences demonstrate that the formation of La-B phases allows $NaBH_4$ to decompose and regenerate under moderate conditions. The participation of F^- in the $NaBH_4$+LaF_3 system results in a further reduction of the desorption enthalpy change of $NaBH_4$, and thereby further decreases the onset dehydrogenation temperature and improves the dehydrogenation kinetics of $NaBH_4$.

4. Conclusions

In the present work, two $NaBH_4$ based reversible hydrogen storage composites, namely, $NaBH_4$+LaH_2 and $NaBH_4$+LaF_3 systems, were prepared via mechanical milling $NaBH_4$ with La and LaF_3 under argon atmosphere, respectively. The hydrogen de-/absorption thermodynamic and kinetic properties, the de-/rehydriding cyclic performance and reaction mechanisms as well as dehydrogenation nucleation modes of the two systems were systematically investigated. Based on the theoretical and experimental analyses, the following conclusions can be drawn:

1. The desorption and absorption enthalpies (ΔH) of the $NaBH_4$+LaF_3 system obtained by PCT measurements are 72.5 and -31.8 kJ mol^{-1} H_2, respectively. The desorption enthalpy of the $NaBH_4$+LaH_2 system is calculated to be 89.6 kJ mol^{-1} H_2 by DSC measurement. The difference in desorption enthalpy of $NaBH_4$+LaF_3 to $NaBH_4$+LaH_2 system could be ascribed to the appearance of thermodynamically more stable compound NaF compared to NaH. In case of the 1st dehydrogenation, the onset dehydrogenation temperature is decreased from 517 °C for pristine $NaBH_4$ to 160 °C for $NaBH_4$+LaF_3 sample, and 330 °C for $NaBH_4$+LaH_2 sample.

2. The much faster dehydrogenation kinetics of the $NaBH_4$+LaF_3 sample than that of the $NaBH_4$+LaH_2 sample may be ascribed to the different nucleation modes. Analyses using JMA model indicate a nucleation-site saturation mode with nucleation occurred at the grain corners for the $NaBH_4$+LaF_3 system, while a random nucleation mode with early nucleation at dislocations or highly anisotropic of growth velocities is found for the $NaBH_4$+LaH_2 system. The apparent dehydrogenation activation energies (E_a) are calculated to be 220.1 and 247.0 kJ mol^{-1} for $NaBH_4$+LaF_3 and $NaBH_4$+LaH_2 systems, respectively.

3. Re-/dehydriding cyclic measurements reveal that the hydrogen storage capacities during six cycles are in the range of 3.02-3.53 wt% for the $NaBH_4$+LaF_3 system, and 3.02-3.41 wt% for the $NaBH_4$+LaH_2 system. The temperatures at which the maximum dehydrogenation rates are achieved are lowered down in both

systems after de-/rehydrogenation cycles. After six re-/dehydrogenations, the desorption products of $NaBH_4$+LaF_3 and $NaBH_4$+LaH_2 samples could be rehydrogenated at 238 ^oC and 326 ^oC with hydrogen storage capacity of 3.0 wt% and 2.9 wt%, respectively. The remarkable improvement in de-/absorption kinetics obtained through cycling could be attributed to the size reduction of $NaBH_4$ particles achieved by cycling in both systems and the formation of the $NaBF_{4-x}H_x$ complex phase in the $NaBH_4$+LaF_3 system.

4. Phase examinations demonstrate that LaB_6 is one product of the reaction between $NaBH_4$ and LaF_3, while LaB_4 is the product of reaction between $NaBH_4$ and LaH_2. Both LaB_6 and LaB_4 enable the regeneration of $NaBH_4$ at moderate conditions. XPS analyses demonstrate that the function anion F^- acts as substitutional anion for H^- to yield $NaBF_{4-x}H_x$ and $NaF_{1-x}H_x$ during de-/rehydrogenation processes in the $NaBH_4$+LaF_3 system. According to a series of designed experiments and results of phase analyses, the observed better promotion effects of LaF_3 over LaH_2 on the hydrogen sorption reversibility of $NaBH_4$ can be ascribed to: i) F^- anion favors the formation of LaB_6 while H^- favors the formation of LaB_4; ii) The formation of NaF instead of NaH further reduces the enthalpy gap between reactants and products; iii) The F^- participates in the re-/dehydrogenation of $NaBH_4$ as a substitutional anion for H^-, resulting in more favorable hydrogen sorption thermodynamics and kinetics.

Acknowledgements

Prof. Zou would like to thank the support from the Science and Technology Committee of Shanghai under Nos. 10JC1407700 and 11ZR1417600, and 'Pujiang' project (No. 11PJ1406000). This work is partly supported by Research Fund for the Doctoral Program of Higher Education of China (No. 20100073120007) and from the Shanghai Education Commission (No. 12ZZ017).

References

1. M. S. Dresselhaus and I. L. Thomas, *Nature,* 2001**, 414**, 332-337.
2. S. Orimo, Y. Nakamori, J. R. Eliseo, A. Zuttel and C. M. Jensen, *Chem. Rev.,* 2007, **107**, 4111-4132.
3. F. Schuth, B. Bogdanovic and M. Felderhoff, *Chem. Commun.,* 2004, 2249-2258.
4. P. Ngene, R. van den Berg, M. H. W. Verkuijlen, K. P. de Jong and P. E. de Jongh, *Energy Environ. Sci.,* 2011, **4**, 4108-4115.
5. S. Orimo, Y. Nakamori and A.Zuttel, *Mater. Sci. Eng. B,* 2004, **108**, 51-53.
6. L. N. Chong, J. X. Zou, X. Q. Zeng and W. J. Ding, *J. Mater. Chem. A,* 2013**, 1**, 3983-3991.
7. L. N. Chong, J. X. Zou, X. Q. Zeng and W. J. Ding, *J. Mater. Chem. A,* 2013**, 1**, 13510-13523.
8. J. X. Zou, L. J. Li, X. Q. Zeng and W. J. Ding, *Int. J. Hydrogen Energy,* 2012, **37**, 17118-17125.
9. J. F. Mao, Z. P. Guo, I. P. Nevirkovets, H. K. Liu and S. X. Dou, *J. Phys. Chem. C,* 2012, **116**, 1596-1604.
10. R. Cerny, G. Severa, D. B. Ravnsbæk, Y. Filinchuk, V. D'Anna, H. Hagemann, D. Haase, C. M. Jensen and T. R. Jensen, *J. Phys. Chem. C,* 2010, **114**, 1357-1364.
11. J. Urgnani, F. J. Torres, M. Palumbo and M. Baricco, *Int. J. Hydrogen Energy,* 2008, **33**, 3111-3115.
12. H.-W. Li, S. Orimo, Y. Nakamori, K. Miwa, N. Ohba, S. Towata and A. Züttel, *J. Alloys Compd.,* 2007, **446–447**, 315-318.
13. D. Ravnsbæk, Y. Filinchuk, Y. Cerenius, H. J. Jakobsen, F. Besenbacher, J. Skibsted and T. R. Jensen, *Angew. Chem. Int. Ed.,* 2009, **48**, 6659-6663.
14. G. Xia, L. Li, Z. Guo, Q. Gu, Y. Guo, X. Yu, H. Liu and Z. Liu, *J. Mater. Chem. A,* 2013, **1**, 250-257.
15. V. D'Anna, L. M. L. Daku, H. Hagemann and F. Kubel, *Phys. Rev. B: Condens. Matter Mater. Phys.,* 2010, **82**, 024108.
16. H. W. Brinks, A. Fossdal and B. C. Hauback, *J. Phys. Chem. C,* 2008, **112**, 5658-5661.
17. N. Eigen, U. Bosenberg, J. B. von Colbe, T. R. Jensen, Y. Cerenius, M. Dornheim, T. Klassen and R. Bormann, *J. Alloys Compd.,* 2009, **477**, 76-80.
18. L. C. Yin, P. Wang, X. D. Kang, C. H. Sun and H. M. Cheng, *Phys. Chem. Chem. Phys.,* 2007, **9**, 1499-1502.
19. L. C. Yin, P. Wang, Z. Z. Fang and H. M.Cheng, *Chem. Phys. Lett.,* 2008, **450**, 318-321.
20. J. J. Vajo, S. L. Skeith and F. Mertens, *J. Phys. Chem. B,* 2005, **109**, 3719-3722.
21. S. Garroni, C. Pistidda, M. Brunelli, G. B. M. Vaughan, S. Surinach and M. D. Baro, *Scr. Mater.,* 2009, **60**, 1129-1132.
22. C. Milanese, S. Garroni, A. Girella, G. Mulas, V. Berbenni, G. Bruni, S. Surinach, M. D. Baro and A. Marini, *J. Phys. Chem. C,* 2011, **115**, 3151-3162.
23. J.-H. Shim, J.-H. Lim, S.-u. Rather, Y.-S. Lee, D. Reed, Y. Kim, D. Book and Y. W. Cho, *J. Phys. Chem. Lett.,* 2010, **1**, 59–63.
24. F. C. Gennari, *Int. J. Hydrogen Energy,* 2011, **36**, 15231-15238.
25. F. C. Gennari, L. F. Albanesi, J. A. Puszkiel and P. A. Larochette, *Int. J. Hydrogen Energy,* 2011, ***36***, 563-570.
26. P. Mauron, M. Bielmann, A. Remhof, A. Züttel, J.-H. Shim and Y. W. Cho, *J. Phys. Chem. C,* 2010, **114**, 16801–16805.
27. A. Kato, M. Katayama, A. Mizutani, N. Ito and T. Hattori, *J. Appl. Phys.,* 1997, **81**, 445-450.
28. L. M. Kulikov, V. I. Lazorenko and G. V. Lashkarew, *Powder Metall. Met. Ceram.,* 2002, **41**, 107-111.
29. L.-P. Ma, X.-D. Kang, H.-B. Dai, Y. Liang, Z.-Z. Fang, P.-J. Wang, P. Wang and H.-M. Cheng, *Acta Mater.,* 2009, **57**, 2250-2258.
30. S. V. Meschel and O. Kleppa, J. *J. Alloys Compd.,* 2001, **321**, 183-200.
31. S. A. Jin, J. H. Shim, Y. W. Cho, K. W. Yi, O. Zabara and M. Fichtner, *Scr. Mater.,* 2008, **58**, 963-965.
32. A. Roine, *Outokumpu HSC Chemistry for Windows: Chemical Reaction and Equilibrium Software with Extensive Thermodynamical Database and Flowsheet Simulation,* Version 6.0. 06120-ORC-T, Outokumpu Research Oy, Finland, 2006.
33. M. Au, A. Jurgensen and K. Zeigler, *J. Phys .Chem. B,* 2006, **110**, 26482-26487.
34. Z. Z. Fang, X. D. Kang, P. Wang and H. M. Cheng, *J. Phys. Chem. C,* 2008, **112**, 17023-17029.
35. M. Au, A. R. Jurgensen, W. A. Spencer, D. L. Anton, F. E. Pinkerton, S. J. Hwang, C. Kim and R. C. Bowman, *J. Phys. Chem. C,* 2008, **112**, 18661-18671.

36. M. Au and A.Jurgensen, *J. Phys. Chem. B,* 2006, **110**, 7062-7067.
37. J. Xu, X. B. Yu, J. Ni, Z. Q. Zou, Z. L. Li and H. Yang, *Dalton Trans.,* 2009, **39**, 8386-8391.
38. G. Xia, Q. Meng, Z. Guo, Q. Gu, H. Liu, Z. Liu and X. Yu, *Acta Mater.,* 2013, **61**, 6882-6893.
39. O. Kircher and M. Fichtner, *J. Alloys Compd.,* 2005, **339**, 404–406.
40. D. Blanchard, H. W. Brinks and B. C. Hauback, *J. Alloys Compd.,* 2006, **416**, 72-79.
41. M. Avrami, *J. Chem. Phys.,* 1939, **7**, 1103-1112.
42. Y. F. Liu, F. H. Wang, Y. H. Cao, M. X. Gao, H. G. Pan and Q. D. Wang, *Energy Environ. Sci.,* 2010, **3**, 645-653.
43. J. W. Christian, *The Theory of transformations in metals and Alloys, 2nd ed., Pergamon: New York,* 1975.
44. W. Z. Zhu, T. C. Lei and Y. Zhou, *Ceram. Int.,* 1994, **20**, 105-109.
45. C. Bonatto Minella, S. Garroni, C. Pistidda, R. Gosalawit-Utke, G. Barkhordarian, C. Rongeat, I. Lindemann, O. Gutfleisch, T. R. Jensen, Y. Cerenius, J. Christensen, M. D. Baró, R. Bormann, T. Klassen and M. Dornheim, *J. Phys. Chem. C,* 2011, **115**, 2497-2504.
46. E. Deprez, M. A. Munoz-Marquez, M. A. Roldan, C. Prestipino, F. J. Palomares, C. B. Minella, U. Bosenberg, M. Dornheim, R. Bormann and A. Fernandez, *J. Phys. Chem. C,* 2010, **114**, 3309-3317.
47. R. Gosalawit-Utke, J. M. Bellosta von Colbe, M. Dornheim, T. R. Jensen, Y. Cerenius, C. B. Minella, M. Peschke and R. Bormann, *J. Phys. Chem. C,* 2010, **114**, 10291-10296.
48. S.-A. Jin, Y.-S. Lee, J.-H. Shim and Y. W. Cho, *J. Phys. Chem. C,* 2008, **112**, 9520-9524.
49. G. Barkhordarian, T. Klassen, M. Dornheim and R. Bormann, *J. Alloys Compd.,* 2007, **440**, L18-L21.
50. M. Dornheim, S. Doppiu, G. Barkhordarian, U. Bosenberg, T. Klassen, O. Gutfleisch and R. Bormann, *Scr. Mater.,* 2007, **56**, 841-846.
51. C. P. Balde, B. P. C. Hereijgers, J. H. Bitter and K. P. de Jong, *J. Am. Chem. Soc.,* 2008, **130**, 6761-6765.
52. W. Lohstroh, A. Roth, H. Hahn and M. Fichtner, *Chem. Phys. Chem.,* 2010, **11**, 789-792.
53. J. Yang, A. Sudik and C. Wolverton, *J. Phys. Chem. C,* 2007, **111**, 19134-19140.
54. H. Yang, A. Ibikunle and A. J. Goudy, *Adv. Mater. Sci. Eng.,* 2010, doi:10.1155/2010/138642.
55. J. F. Mao, X. B. Yu, Z. P. Guo, H. K. Liu, Z. Wu and J. Ni, *J. Alloys Compd.,* 2009, **479**, 619-623.
56. J. F. Mao, Z. P. Guo, X. B. Yu and H. K. Liu, *J. Phys. Chem. C,* 2011, **115**, 9283-9290.
57. G. Renaudin, K. Yvon, W. Wolf and P. Herzig, *J. Alloys Compd.,* 2005, **404-406**, 55-59.
58. J. H. Shim, J. H. Lim, S. U. Rather, Y. S. Lee, D. Reed, Y. Kim, D. Book and Y. W. Cho, *J. Phy. Chem. Lett.,* 2010, **1**, 59-63.
59. R. E. Thoma, *Inorg. Chem.,* 1962, **1**, 220-226.
60. J. F. Moulder, W. F. Stickle, P. E. Sobol and K. D. Bomben, *In Handbook of X-ray Photoelectron Spectroscopy;* Perkin-Elmer Corp., Eden Prairie, MN 1992.
61. E. H. Majzoub, J. L. Herberg, R. Stumpf, S. Spangler and R. S. Maxwell, *J. Alloys Compd.,* 2005, **394**, 265.

graphical abstract

Both LaF_3 and the in situ formed LaH_2 enable the reversible hydrogen sorption in $NaBH_4$. Systematic studies show that the formation of La-B phases in dehydrogenation products of the two composites plays the major role for the reversible hydrogen sorption in $NaBH_4$. In particular, the regeneration of $NaBH_4$ can be achieved at 238 ^oC for the $NaBH_4$+LaF_3 composite, and 326 ^oC for the $NaBH_4$+LaH_2 composite after 6 dehydrogenation cycles. Comparative studies demonstrate that the substitution of F^- for H^- yields $NaBH_{4-x}F_x$ and $NaF_{1-x}H_x$ phases during de-/rehydrogenation processes in the $NaBH_4$+LaF_3 composite, resulting in more favorable thermodynamics.

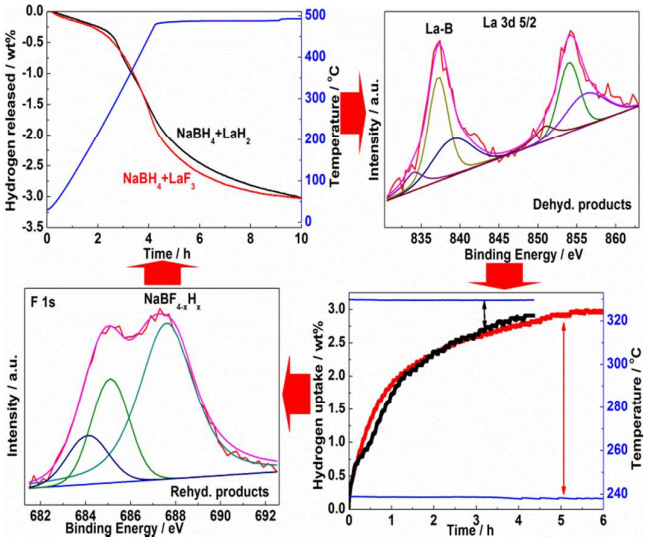

Lina Chong [a], Jianxin Zou [a,b*], Xiaoqin Zeng [a,b], Wenjiang Ding [a,b]

< Effects of La fluoride and La hydride on the reversible hydrogen sorption behaviors in $NaBH_4$: A comparison study >